# PARAMETERIZATION AND SCALING OF ARCTIC ICE CONDITIONS IN THE CONTEXT OF ICE-ATMOSPHERE PROCESSES



NASA GRANT NAGW-2598

YEAR 3 ANNUAL REPORT

September 1994

Investigators:

R. G. Barry (PI)
J. Heinrichs
K. Steffen
J. A. Maslanik
J. Key
M. C. Serreze
R. W. Weaver

Cooperative Institute for Research in Environmental Sciences
Division of Cryospheric and Polar Processes
University of Colorado
Boulder, CO 80309-0449

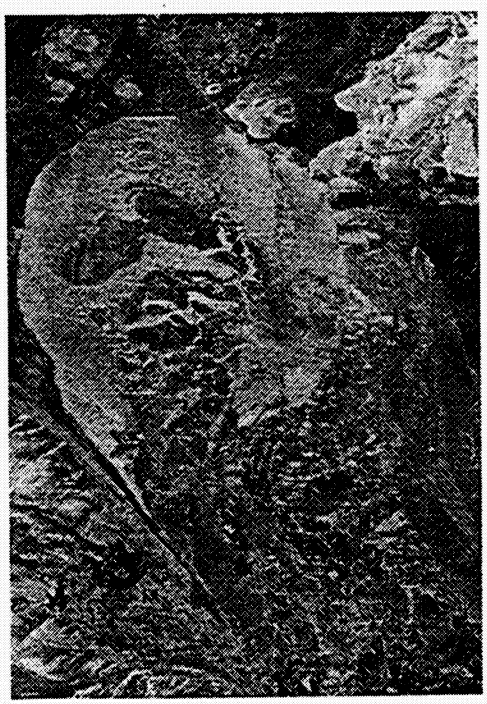

TABLE OF CONTENTS

# 1. INTRODUCTION AND EXECUTIVE SUMMARY

This report summarizes achievements during year 3 of our project to investigate the use of ERS-1 SAR data to study Arctic ice and ice/atmosphere processes. The project was granted a one year extension at no cost, and this report outlines our goals during the final year. The final report will be delivered in October 1995.

## 1.1 Project Objectives

The specific objects of the project are to:

- determine how the development and evolution of open water/thin ice areas within the interior ice pack vary under different atmospheric synoptic regimes;

- compare how open water/thin ice fractions estimated from large-area divergence measurements differ from fractions determined by summing localized openings in the pack;

- relate these questions of scale and process to methods of observation, modeling, and averaging over time and space;

- determine whether SAR data might be used to calibrate ice concentration estimates from medium and low-rate bit sensors (AVHRR and DMSP-OLS) and the Special Sensor Microwave/Imager (SSM/I); and

- investigate methods to integrate SAR data for turbulent heat flux parametrization at the ocean/atmosphere interface with other satellite data.

## 1.2 Year 3 Progress

Major accomplishments over year 3 included:

- The SAR-based ice classification work performed in the previous two years has been completed. The general effectiveness of SAR ice type classification was assessed by comparison with Landsat TM data, and a specific evaluation of the performance of the ice type classifier used operationally by the Geophysical Processing System (GPS).

- Major insights have been gained into the seasonal cycle of typical pack ice and how that cycle is reflected in SAR imagery. By a detailed qualitative examination, and the development and evaluation of a simple numerical/backscatter model, we are able to identify major features of the seasonal cycle and describe their appearance in SAR data.

- As a consequence of the above, a time series of mean SAR backscatter through the year was used as a means of evaluating both other remote sensing products (SSM/I) and a commonly used physical model of ice processes.

- A simple method for using SAR data for determining ice concentration was developed. By taking the effects of wet snow and meltponds into account, this method can be used to estimate the fractions of different ice types throughout the year. Although no *in situ* data was available for validation, the concentrations obtained from this method appear reasonable when compared with those from other sources.

- A study of the Lady Ann Strait polynya using SAR imagery was conducted in which we learned how to interpret SAR imagery in the dynamic and sometimes confusing polynya environment and examined the change of backscatter with time on both short and long temporal scales.

- In conjunction with a separate NASA grant, SAR imagery and SAR-derived ice motions were combined with AVHRR-derived ice motions, SSM/I data and sea-ice model output to study the relationships between observed ice concentrations and simulated divergence and shear during October 1991 and extended through May 1992 for the Beaufort Sea. No large descrepancies were found between simulated changes in concentration and those observed in the imagery. However, the SSM/I data suggest substantially larger increases in first-year ice fraction, which might be related to sub-time-step changes in open water coverage. Significant correlations exist between changes in SSM/I-derived ice concentration and simulated divergence and shear over about 40% of the study area.

## 1.3 Year 4 Plans

During year 4 we intend to pursue the following activities:

- The study of the seasonal cycle of pack ice using SAR data will be continued. A particular objective will be to vary the assumptions used in the numerical/backscatter model. Further efforts will be made to use the SAR time series as a tool for evaluating models and data from other sensors.

• The Lady Ann Strait and North Water polynya studies will be pursued further. Objectives will be to determine the typical evolutionary sequences of the polynya as a whole preparatory to a comparison with predicted ice growth and dynamics from a coupled ice/ocean polynya model.

• Comparison of SAR and AVHRR-derived ice motions, SAR lead patterns, SSM/I ice concentrations, and model simulations will be expanded to include the period from June 1992 - June 1993, in conjunction with separate NASA funding.

## 2. YEAR 3 ACTIVITIES

### 2.1 Ice type classification

During the past year, we improved and consolidated our previous work on SAR-based ice type classification using Landsat TM data as "truth". A more careful selection of training data regions was made and the coregistration, calibration and statistics processing improved and streamlined. Our study of ice typing, which has been described in a paper currently in press (Steffen and Heinrichs 1994a), had two major objectives. The first was to evaluate SAR-based ice typing in general using Landsat TM data, and the second and more specific was to assess the performance of the operational classifier used in the Geophysical Processing System (GPS) at the Alaska SAR Facility (ASF).

The data set used in our work consisted of two overlapping pairs of Landsat TM and ERS-1 SAR images taken on April 15 and 18, 1992 covering a portion of the Beaufort Sea centered at 145° W, 73° N. The Landsat data was obtained from EOSAT Corporation and was geolocated, mapped to the UTM projection, and gridded to 25 m spatial resolution (slightly better than the actual 30 m resolution) in order to better match the SAR. Data from the C-band (5.3 GHz) SAR instrument aboard ERS-1 was obtained from the ASF at its full 12.5 m spatial resolution, resampled to 25 m resolution, and mapped to the UTM projection. Coregistration of the image pairs was a challenging process, given both the movement of the ice and certain errors in the data processing of the SAR, and was accomplished by the use of successively smaller offsets determined visually and the use of color composite images for precise registration.

Once coregistration and image subsetting were complete, images of TM band 4 (760-900 nm) and, occasionally, TM band 6 (10.4 - 12.5 mm in the thermal infrared) were used to select training data regions for each of seven ice types as defined by the standard WMO nomenclature. We accumulated training data areas until a sufficient sample size (roughly 1000 points) was attained for each type. The training data were used to define a supervised classification (maximum likelihood) based on Landsat TM band 4.

Table 1 shows the results of our statistical analysis of the SAR pixels assigned to each ice type as defined by the Landsat supervised classification. A graphical representation of these results is shown in Figure 1. The TM data shows a distinct separation between most ice classes with, however, some overlap between first year ice (FYI) and old ice (OI). This is due to the snow cover over both ice types causing their albedos to be very similar. The SAR data, however, shows major overlaps between many ice types. OI and FYI can be readily distinguished in the SAR data, but the nilas (NI), grey ice, and grey-white ice categories have substantial overlap, both with each other and with the OI and FYI classes. The ice free (IF) areas also have

backscatter values similar to the solid ice types, but different for the two days studied. This is a consequence of wind roughening (increased backscatter caused by wind-formed capillary waves on the ocean surface). Wismann (1993) has provided a formula which relates the backscatter of IF areas backscatter to wind speed ($\sigma^0_{IF} = 0.0785u^{0.781604}$, where $\sigma^0_{IF}$ is the backscatter of the ice free surface and u is the wind speed). The observed backscatter from ice free areas is slightly less than what would be expected from this relationship, but does show a higher backscatter on April 18 when winds were stronger. We hypothesize that the Wismann formula is more appropriate for larger open ocean areas then the leads found in the pack ice environment.

Table 1. Derived SAR backscatter coefficient ($\sigma^\circ$) statistics (mean and standard deviation) by ice type based on the supervised ice type classification from Landsat Thematic Mapper channel 4 for the Beaufort Sea (April 16 and 18, 1992).

| | April 16, 1992 Backscattering Coefficient (dB) | | April 18, 1992 Backscattering Coefficient (dB) | |
|---|---|---|---|---|
| Ice Type | Mean | SD | Mean | SD |
| IF | -15.12 | 3.28 | -5.31 | 1.95 |
| NI | -12.35 | 4.03 | -10.39 | 3.95 |
| GI | -14.01 | 2.98 | -13.14 | 2.38 |
| GWI | -15.17 | 3.53 | -14.25 | 2.99 |
| FYI-I | -16.26 | 4.67 | -16.75 | 3.23 |
| FYI-II | -17.41 | 4.87 | -16.70 | 3.69 |
| OI | -10.97 | 3.43 | -10.20 | 2.47 |

Figure 1. Graph showing means and standard deviations of Landsat TM band 4 spectral radiance and SAR backscatter coefficient for each of seven ice types.

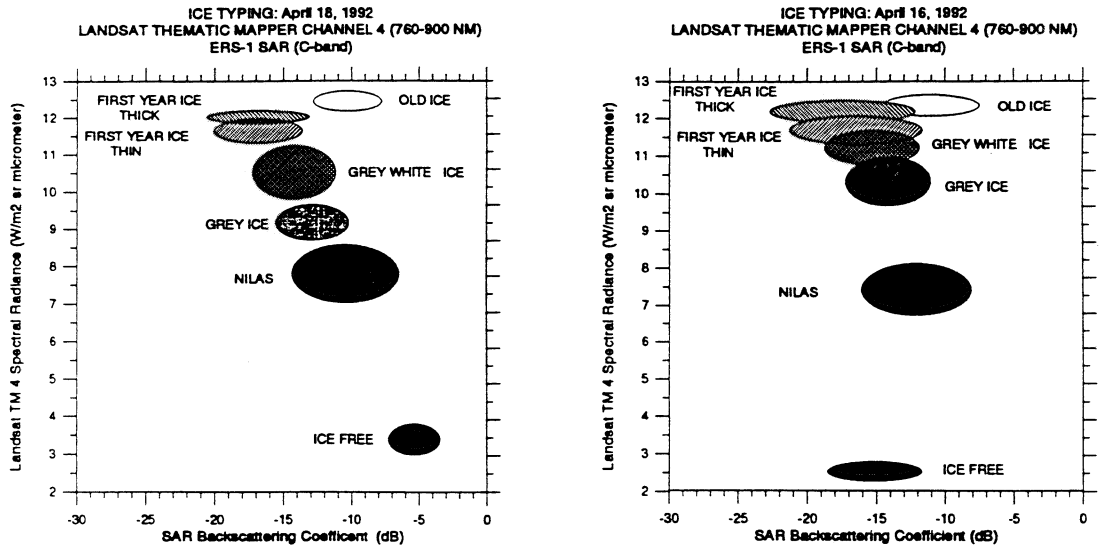

Our evaluation of the GPS classifier was based on the results of the SAR/Landsat comparison described above. The GPS ice types are somewhat different from the WMO list (Kwok and Cunningham 1992, Kwok et al 1992), and the training data was recombined to reflect this difference. Table 2 lists the SAR means and standard deviations for each of the categories as defined by the GPS and the TM supervised classification for April 16. While, the two classifications agree well for FYI-I and OI, significant differences in the means exist for the combined IF/NI/YI and the FYI-II classes. The GPS threshold used for IF generally restricts identification to calm wind conditions. IF areas identified in the TM imagery, because of the moderate winds on April 16, have higher backscatter values and are misclassified by the GPS as other types. By calculating the percentage of correct decisions made by the GPS classifier as compared to the TM-derived classification, we were able to quantitatively assess the GPS performance. These results are listed in Table 3. As expected from the means and standard deviations, OI classification accuracy is the best of the four GPS types with FYI-I a distant second. IF/NI/YI and FYI-II categories are clearly not performing well, most likely due to misclassification of IF pixels. Ice concentrations were determined for both study dates using SAR and TM thresholds. The TM values are closer to the expected ones, and show the expected relation to divergence (lower concentration on April 18 associated with higher wind speeds). SAR-derived concentrations show the opposite tendency, most likely due to a larger fraction of IF pixels being wind-roughened and misclassified as solid ice.

Table 2. Mean SAR backscatter coefficient and standard deviation (SD) for the GPS ice classifier and the Landsat TM channel 4 based ice classification for ice free, nilas and young ice (IF, NI, YI), thin first-year or smooth first-year ice (FYI-I), medium and thick first-year or deformed first-year ice (FYI-II) and old ice (OI) on April 16, 1992.

| Ice Type | GPS mean | GPS SD | TM mean | TM SD |
|---|---|---|---|---|
| IF, NI, YI | -20.7 | 3.5 | -14.2 | 3.5 |
| FYI-I | -17.8 | 3.9 | -16.3 | 4.7 |
| FYI-II | -14.0 | 3.7 | -17.4 | 4.9 |
| OI | -10.8 | 3.3 | -11.0 | 3.4 |

Table 3. Performance of the GPS SAR ice type classifier. The correctly classified percentage for each SAR ice type as compared to the TM ice classes is given in parentheses. The comparison was done with the co-registered Landsat and SAR images (650,000 pixels) for April 16, 1992. The total percentage of each ice type as derived from TM for the entire image is also given.

| SAR | Landsat TM Channel 4 Ice Classes | | | |
|---|---|---|---|---|
| Ice Classes | IF & YI (0.3 %) | FYI-I (20.8 %) | FYI-II (21.1 %) | OI (57.8 %) |
| IF, NI, YI (%) | (13.6) | 34.9 | 31.2 | 20.3 |
| FYI-I (%) | 11.9 | (36.1) | 27.1 | 24.9 |
| FYI-II (%) | 40.5 | 21.0 | (16.4) | 22.1 |
| OI (%) | 4.4 | 7.2 | 25.8 | (62.6) |

The final portion of the study involved an examination of the effectiveness of using the SAR and TM data together in a multispectral classification. SAR is superior for separating FYI and OI, where Landsat has advantages for IF, NI, and YI. We assembled a set of training data using color composite images of SAR and TM data together to assign a priori categories and evaluated the performance of several channel combinations against the training data. For each channel set investigated, we calculated the parameters for a maximum likelihood classifier, which was then applied to the training data. Accuracy percentages for each category were calculated for each channel set. The combination of SAR and single TM visible channels (channels 2,3, or 4) was found to improve accuracy over TM for all but the FYI types. Adding multiple visible channels improved accuracy for FYI-II, and adding channel 6 (thermal infrared) resulted in an accuracy greater than or equal to 90% for all types.

2.2. Studies of the Seasonal Cycle of Sea Ice Using SAR Data

The potential of SAR data for longer-term monitoring of sea ice has only begun to be explored, despite the important advantages of SAR data for this kind of research. We conducted a study aimed at determining the variation of backscatter with time from typical pack ice and how these changes relate to physical changes in the ice are important problems

The data used in this study covered a region in the Beaufort Sea centered at 78° N, 153° W during a 13-month period from October 1992 to November 1993. A series of 31 images from the ERS-1 C-band SAR was obtained from the Alaska SAR Facility (ASF) and calibrated using the

operational ASF algorithm. As part of the calibration process, the data was scaled from Digital Number (DN) values to backscatter values in dB. In addition to the SAR data, we obtained concurrent meteorological data from the National Meteorological Center (NMC), including surface air temperature, pressure, and geostrophic wind fields. The complete time series is illustrated in Figure 2.

Figure 2. Graph of the mean ERS-1 SAR backscatter and NMC temperature and wind speed data used to study the seasonal cycle of sea ice in the Beaufort Sea. Roman numerals identify the regime (see text for explanation) and vertical lines are regime boundaries.

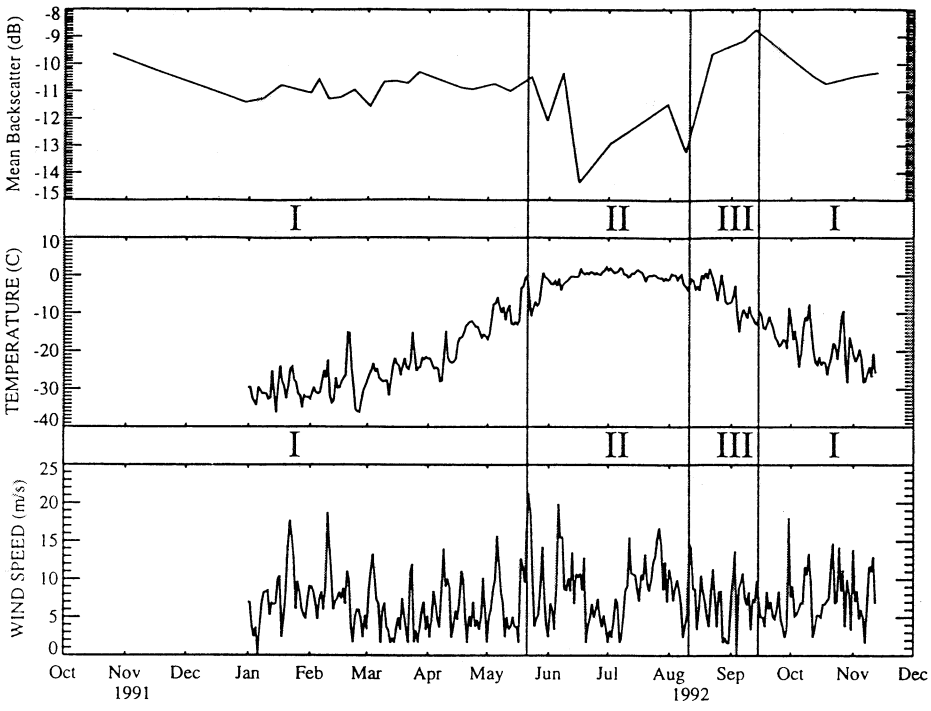


2.2.1 Qualitative Examination

The first general observation we made is that there is substantial variability in the appearance of sea ice throughout the year in SAR imagery. Not only may a given value of backscatter correspond to more than one kind of ice (or even wind-roughened IF), but this relationship changes through the year. Nevertheless, we have segmented the year into three major evolutionary regimes that, we feel, have a consistent set of ice signatures and a correspondence to major features in the seasonal cycle of sea ice.

The first regime we identified (regime I) covers the majority of the year, beginning in autumn and extending all the way through spring until summer melt occurs. The signatures of FYI and

multiyear ice (MYI) are relatively stable, about -16 and -10 dB, respectively. The major modulation of the mean backscatter in the time series was the variations in ice concentration and the wind roughening and corresponding backscatter increases of IF. Beginning shortly before the summer solstice we have another major regime (regime II), in which the appearance of sea ice changes dramatically. First, the snow cover above the ice surface begins to melt. At first, this involves primarily the addition of water to the snow layer. This water, because it is embedded in the snow matrix, is not subject to wind roughening and acts as a very efficient absorber of electromagnetic radiation at radio wavelengths. Because of this, the MYI and FYI have a significantly reduced backscatter. Pressure ridges, which protrude above the layer of wet snow, appear as bright linear features. Later in the summer, the wet snow melts completely, with much of the water collected in meltponds. The meltponds are also subject to wind roughening, and the result is a dramatic increase in the sensitivity of the mean backscatter to wind speed. The floes also become disaggregated. At the end of the summer, the appearance of sea ice in the SAR imagery changes once again, defining the third regime (regime III). MYI regains its normal appearance as the meltponds refreeze, and FYI begins to form once again. The major difference in this regime from the previous regime is the presence of broadly linear bright features. These features have a general appearance similar to that of the IF areas in the summer, and we suspect they are due to the refreezing of the leads with their multitudes of disaggregated floes combining in a jumble of angular fragments which act as reflectors (both direct and via cornering) for radiation at C-band wavelengths.

### 2.2.2 A Simple Ice Cover/backscatter Model

In order to test our hypotheses and the conceptual model that originated during the qualitative examination of the data set, we constructed a simple numerical model. Our plan was to link a simple backscatter model to this numerical model and then compare the resulting backscatter estimates to the actual time series.

We began by assuming ice concentrations to be constant in each regime. This assumption simplifies the initial evaluation of the model and, furthermore, can be changed at any time. The physical characteristics of the model are, as would be expected, dependent on the time of year (using the regimes defined above). In regime I (autumn/winter/spring), we have only FYI, MYI, and IF present (NI, grey ice, and grey-white have been excluded to simplify the model). During the summer, all of the FYI becomes MYI, which is partially covered by wet snow and meltponds. Because of their importance to the energy balance of the ice, and because of their strong effect on the SAR backscatter, we added a more detailed parameterization of their growth. A maximum fraction for snow cover on the ice is chosen, as is a maximum meltpond fraction. These numbers were assumed to be 0.65 and 0.4, respectively. At the beginning of the summer season (defined by the excursions of the surface air temperature above and below 0° C) the entire maximum

fraction of wet snow appears. During the summer, the meltpond fraction is calculated for each image by a simple linear relationship of the day since the beginning of summer and the maximum meltpond fraction. Since the meltpond formation is at the expense of the snow-covered area, the area of snow on a given day is reduced to the maximum meltpond fraction linearly with the number of days since the beginning of the melt season. During the late summer freeze (regime III), no IF is allowed and all of the IF from regime II is assigned to the bright ice (BI) category. Table 4 lists the ice concentration values used for the different regimes in our ice cover model.

Table 4. Surface type fractions (range 0.0 to 1.0) used in ice cover model by regime

| Surface Type | Surface Type Fraction | | |
|---|---|---|---|
| | Regime I | Regime II | Regime III |
| MYI | 0.85 | 0.9 | 0.85 |
| FYI | 0.1 | 0 | 0.1 |
| Bright Ice | 0 | 0 | 0.05 |
| IF | 0.05 | 0.1 | 0 |
| Wet Snow | 0 | varies | 0 |
| Meltponds | 0 | varies | 0 |

On top of this simple model of ice cover through the year we added an equally simple model of the mean backscatter of the scene. The mean backscatter of the scene is, by definition, the average of the backscatter values at each pixel. By segmenting the pixels into types, we can calculate the mean backscatter by adding the backscatter of each type weighted by the fraction of area covered by that type (i.e., the concentration). Including all of the ice surface types described above, we then have:

$$\sigma^0 = A_{MY}\sigma^0_{MY} + A_{FY}\sigma^0_{FY} + A_{IF}\sigma^0_{IF} + A_{BI}\sigma^0_{BI} + A_{MP}\sigma^0_{MP} + A_{WS}\sigma^0_{WS} \qquad (1)$$

where $\sigma^0_{MY}$, $\sigma^0_{FY}$, $\sigma^0_{IF}$, $\sigma^0_{BI}$, $\sigma^0_{MP}$, and $\sigma^0_{WS}$ are the backscatter values for multiyear ice, first-year ice, ice free, bright ice, meltponds, and wet snow respectively. $A_{MY}$, $A_{FY}$, $A_{IF}$, $A_{BI}$, $A_{MP}$, and $A_{WS}$ are the corresponding cover fractions for each type. We assumed that each of the solid ice types has a characteristic backscatter, and that all pixels of that type have that backscatter value. To obtain these values, rather than the rigorous training data selection procedure used for the ice type classification study, we examined the time series and chose what we considered typical

values for each type ($\sigma^0_{MY}$ = -10.5 dB, $\sigma^0_{FY}$ = -16.0 dB, $\sigma^0_{BI}$ = -7.0 dB, and $\sigma^0_{WS}$ = -22.0 dB). We assumed that open leads and meltponds are both subject to wind roughening, so that $\sigma^0_{MP}$ and $\sigma^0_{IF}$ are identical and can be calculated by the Wismann formula described above using the NMC wind speeds. It was assumed that the wind speed is constant over the scene.

Figure 3 shows the results of running the combined ice cover/backscatter model. It can be readily seen that the model reproduces the major features of the seasonal cycle, including the stable backscatter values in the winter and spring, the sudden backscatter drop in summer, and the rise during freezeup. More quantitatively, the RMS difference between the actual and simulated backscatter time series is 1.01 dB, which represents about 6% of the full range of backscatter values observed in nature.Some differences exist, however, particularly on shorter time scales. The simulated backscatter seems to be out of phase with the actual time series during the spring months. This may be a function of short-term variations in ice concentration due to large-scale ice motions or the passage of spring storms and consequent divergence.

Figure 3. Comparison of actual SAR mean backscatter time series with simulated time series from simple ice cover backscatter model, SSM/I NASA team algorithm, and Hibler ice dynamics thermodynamics model.

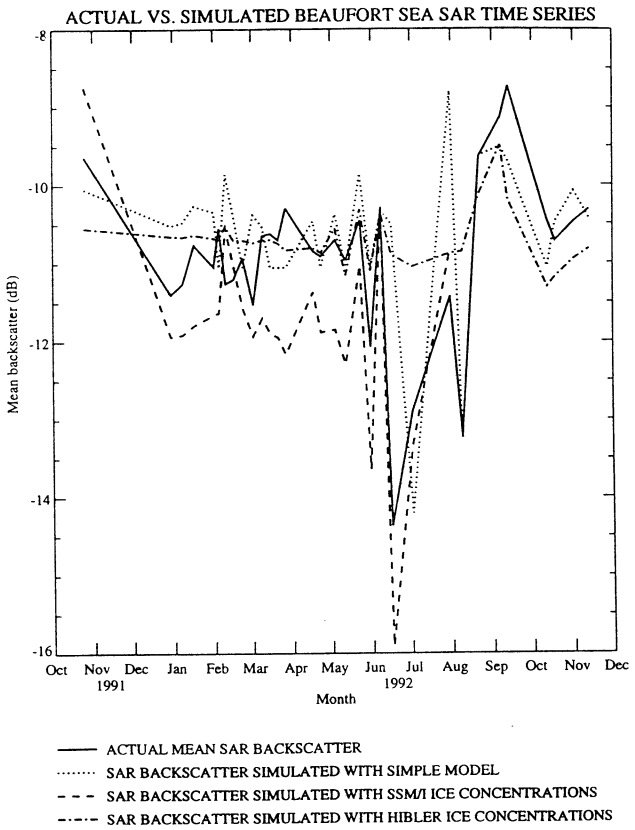

In order to test our simple model, as well as to investigate the use of the backscatter time series as a validation tool in general, we obtained ice concentration estimates for the study area from two other sources. The first was the SSM/I sensor, using the NASA team algorithm with global tie points. The second source was a Hibler ice dynamics/thermodynamics model with viscous-plastic rheology (Hibler 1985), run for the entire Arctic, and from which we extracted the data for the grid point nearest the study area. The Wismann relationship for the backscatter of IF and the backscatter values for the solid ice types were used to calculate mean backscatter from each ice concentration time series. Being a unique feature of our ice cover model, we did not include the effect of meltponds and wet snow in the summer.

Figure 3 also shows the actual SAR time series compared with the simulated SAR data obtained from all three sources (our simple model, the SSM/I NASA team algorithm, and the Hibler model). The SSM/I-derived backscatter estimates are clearly too low, reflecting the generally underestimated concentrations that have been observed using global tie points (Steffen and Schweiger 1990, 1991), but tend to track the changes in the real time series fairly well. The Hibler-derived estimates, on the other hand, have values of about the same overall magnitude as the actual SAR measurements in the winter and spring, but show too little variation all year and particularly in the summer. Table 5 shows the results of a statistical comparison between all three simulated SAR time series and the actual measurements. The lowest RMS error is from the SSM/I, which as mentioned tracks the real time series fairly well, particularly in summer. The Hibler and our simple ice cover models have about the same RMS error (slightly higher than that for the SSM/I), surprising considering the relative complexity of the two. The mean actual/predicted difference is greatest in magnitude for the SSM/I, confirming the observation of a significant bias in the estimates. The mean absolute difference, perhaps the most robust measure of statistical difference in cases where the distribution if non-normal, is almost identical for all three.

Table 5. Error statistics for actual vs. simulated mean SAR backscatter (in dB) for three different sources of simulated SAR.

| Source | RMS Error | Average Error | Average Absolute Error |
|---|---|---|---|
| CU ice cover backscatter model | 1.01 | -0.30 | 0.69 |
| SSM/I NASA team algorithm | 0.69 | 0.51 | 0.66 |
| Hibler ice model | 0.96 | -0.22 | 0.64 |

2.2.3 Ice concentration Algorithm Development

Estimates of ice concentration are useful for both climate research and operational applications (shipping, in particular). During the summer months, when melt occurs and the ice surface undergoes its most dramatic changes, estimates from passive microwave sensors are notoriously inaccurate (to the extent that they are not calculated operationally). The time series analysis described above suggested the a possible approach to obtaining ice concentrations throughout the year from SAR data, with the availability of the NMC meteorological data to help constrain the problem.

At any time the fractional coverage of the various surface types must add to unity. Furthermore, the sum of the backscatter from all sources weighted by the concentration of that ice type must equal the mean backscatter of the scene. Thus we have, assuming the presence of only FYI, MYI, and IF, we have

$$A_{MY} + A_{FY} + A_{IF} = 1 \qquad (2)$$

$$\sigma^0 = A_{MY}\sigma^0_{MY} + A_{FY}\sigma^0_{FY} + A_{IF}\sigma^0_{IF} \qquad (3).$$

By solving for $A_{IF}$ and substituting (2) into (3), we can obtain an equation relating $A_{FY}$ and $A_{MY}$. From our previous work, $\sigma^0_{MY}$ and $\sigma^0_{FY}$ are known ($\sigma^0_{FY} = 0$ in summer). From the NMC wind speeds, and the Wismann formula, $\sigma^0_{IF}$ can be calculated.

We begin calculation of ice concentration by counting the number of pixels with backscatter values above and below a FYI/MYI threshold (-13.5 dB) and obtain $A_{FY(measured)}$ and $A_{MY(measured)}$. Because the entire range of possible backscatter values has been divided into FYI and MYI, the IF points must fall into one of the two classes. Since $\sigma^0_{IF}$ is known, we can decide in which ice type the water points have been included. The other type can then be assumed to be free of IF points and thus exact (i.e., $A_{FY} = A_{FY(measured)}$ or $A_{MY} = A_{MY(measured)}$). Since we have an equation relating $A_{FY}$ and $A_{MY}$, we now know both, and calculation of $A_{IF}$ is a simple matter of substitution.

Figure 4 shows the ice concentrations calculated using this method compared with those from the

SSM/I sensor and Hibler model. It can be observed readily that SSM/I concentration values for MYI are too low, and dramatically so in the summer, when operational ice concentration estimates are not produced. In general, the SAR-derived concentrations are closer to those obtained from the Hibler model than the SSM/I, and certainly fall in the reasonable range. A detailed statistical evaluation has not been performed so far, due to the preliminary and exploratory nature of this work. Potential problems with our approach include errors when the wind speed is close to the threshold value used to separate FYI from MYI (perhaps not significant given the very narrow range of wind speeds yielding such backscatter values).

Figure 4. Ice concentrations obtained from SAR algorithm, NASA team algorithm (SSM/I) and Hibler model.

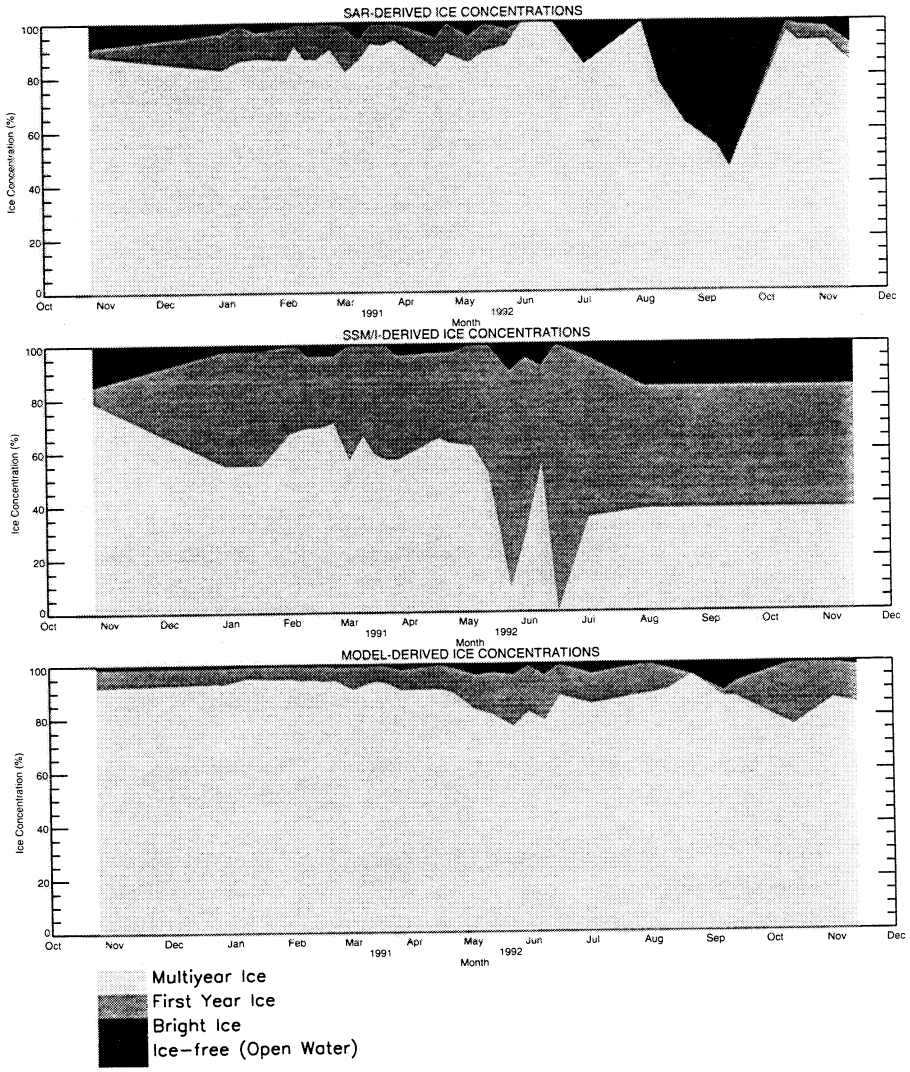

## 2.3. Lady Ann Strait Polynya Study

It is becoming more widely realized that coastal polynyas have a major influence on the heat and energy balance of the ice-covered seas. Furthermore, the large rates of ice formation and brine production typical of polynyas are important climatic factors. Our objective was to examine ice cover variations and the underlying physical processes in one polynya, making use of the rapid repeat coverage during the ERS-1 ice cycle and the SAR instrument's high resolution and ability to penetrate clouds and darkness. Because of extensive previous study, and high suitability for SAR observation, we chose the recurring polynya located in Lady Ann Strait at the mouth of Jones Sound in northwestern Baffin Bay as our subject.

We obtained, from ASF, a series of 30 images of the Lady Ann Strait region covering a period of 5 months between Nov. 20, 1991 and April 17, 1992. The images were of the low resolution product, with 100 m resolution, each 100 km on a side. The images were calibrated using the standard GPS technique, converted to decibels (dB), and scaled.

As can be seen from Figure 5, the appearance of the polynya goes through dramatic changes on short time scales. The Feb. 6 image shows the polynya filled with brash ice composed of broken new ice. Three days later enough ice has formed to cover the polynya, and by the next image this cover has broken up as well. A few relatively large YI floes are visible. By February 15, all of this material has been removed by wind action and ice is again beginning to form. A more detailed understanding of the kinds of ice visible in the SAR images was obtained by taking transects through selected areas of the polynya and examining the backscatter values along the transects. One such profile (taken from the February 6 image) is shown in Figure 6. From this profile, as well as others, we have noted an approximately linear increase of backscatter with ice thickness for new ice and NI.

Figure 5. ERS-1 SAR images of the Lady Ann Strait polynya taken on four days during the study period.

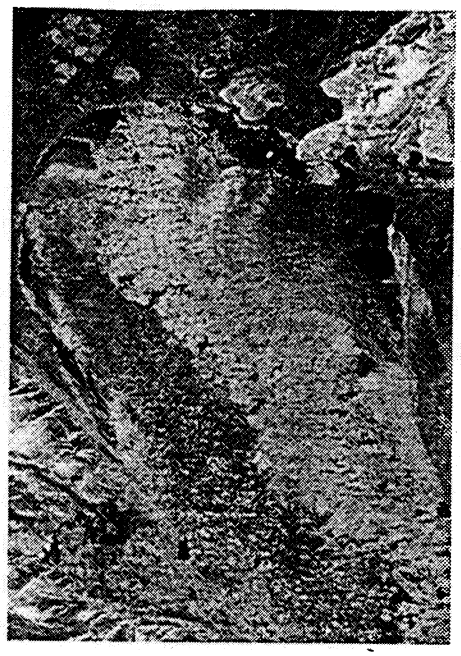

**Feb. 6, 1992**

**Feb. 9, 1992**

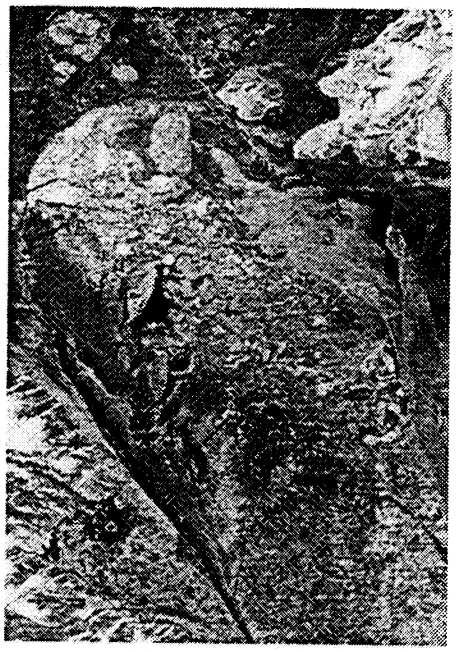

**Feb. 12, 1992**

**Feb. 15, 1992**

Figure 6. Backscatter profile taken across portion of Lady Ann Strait Polynya on February 6, 1992.

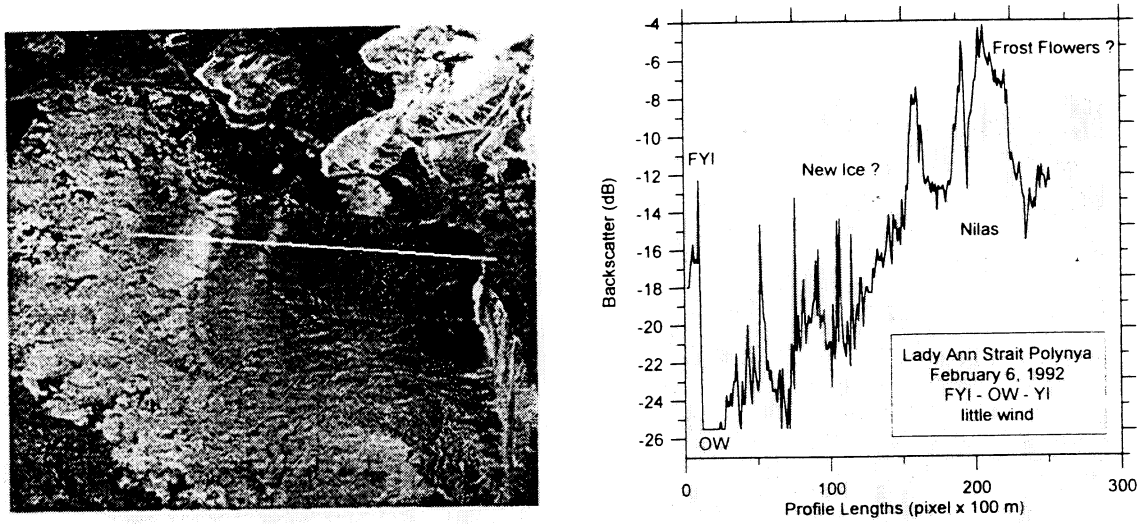


By taking profiles across stable FYI and MYI through the duration of the study period, we were able to examine the temporal change of backscatter with time over longer time scales. Figure 7 shows the results of this analysis. The MYI floes embedded in the FYI matrix show virtually no change in the backscatter, and neither does the smooth FYI. For FYI in general, however, as well as new ice at the ice arch,a distinct downward trend in the backscatter is observed. At present, we do not have a rigorous explanation for these trends.

Figure 7. Sea ice backscatter time series derived from ERS-1 SAR profiles for the Lady Ann Strait polynya.

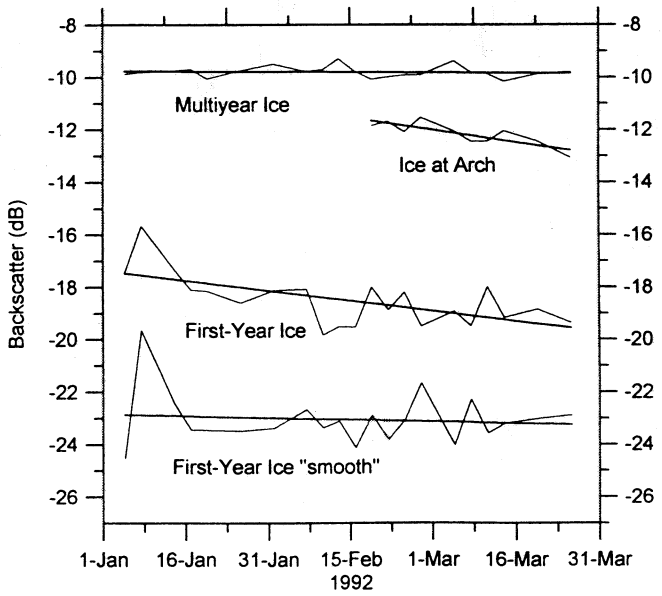

The first conclusion that we can draw from our work on the Lady Ann Strait polynya is a negative one. We do not feel it is possible to obtain ice motions within polynyas from ERS-1 SAR data. The ice orbit of 3 days does not allow ice dynamics to be resolved. Ice velocities within the Lady Ann Strait polynya frequently reach 20 km/day, and can attain 50 km/day (Ito, 1981). In a 3 day period, the ice within the polynya can travel 60 -150 km and move completely outside the boundaries of a 100 km square ERS-1 scene. Radarsat should provide sufficient temporal resolution to allow accurate measurement of polynya dynamics.

Despite the difficulty in resolving ice motions, the SAR data has allowed us to observe the variability of ice cover in the polynya over a relatively long time period. Although much interpretation of the SAR imagery is required in order to assess the ice conditions within the polynya, the high spatial and temporal resolution of our data set makes it a valuable resource. By examining backscatter values along transects within the polynya, we have gained further understanding of the way in which backscatter varies with ice growth for very young ice.

The work described above is a vital step towards the ultimate goal of being able to monitor the ice cover within polynyas and thus determining their heat and energy balances and influences at local, regional, and global scales. Techniques have been developed (ice classification by profile, for example) that will be invaluable for polynya study when more suitable data sets become available. A paper describing our study of the Lady Ann Strait polynya is in preparation and will be submitted shortly to the Journal of Geophysical Research (Steffen and Heinrichs 1994b).

2.4 Response of the Ice Pack to Atmospheric Synoptic Systems

Ice concentrations retrieved from SAR, SSM/I, and AVHRR imagery and simulated using a dynamic-thermodynamic ice model were compared in relation to the passages of strong atmospheric low-pressure systems in the western Arctic for a case study in October 1991, and for a time series through May 1992. Combining different image types and ice model output to study ice conditions allows us to minimize some of the uncertainty in the different data types, and carries more confidence in the interpretation of actual conditions. Since the term "ice concentration" can represent different conditions as defined for different sensors and models, care is needed when intercomparing data sets.

With this caveat in mind, magnitudes of changes in ice concentration as depicted in SSM/I and model output agree reasonably well in the case study for the October (including AVHRR) and over the autumn, winter, and spring period into summer 1992 (SAR, SSM/I, and model output only), showing a 3-5% reduction in ice concentration during the passage of strong storm systems.

SAR imagery shows some evidence of increased lead development and/or opening during passage of the systems, but the total increase in IF/thin ice fraction amounts to only an additional 1 to 2%. AVHRR imagery show greater numbers of leads than are seen in the SAR data, but none of the data sets indicate a large-scale disruption of the ice cover such as has been seen in late summer cases (e.g., Barry and Maslanik, 1989). The largest changes in the ice pack are indicated as an increase in first-year ice fraction in the SSM/I data and model output, which is consistent with refreezing of newly-formed IF areas under diverging and/or shearing conditions. All the data types agree within a few percent for means of total concentration during the autumn through spring period. Disagreement is substantial among the estimated proportions of first-year and multiyear ice.

Differences in simulated concentrations between the runs using viscous-plastic and cavitating fluid rheologies results from the apparent tendency for the cavitating fluid rheology (used here without a representation of shear strength) to overestimate drift speeds relative to a viscous-plastic rheology during periods of rapid ice drift. When averaged over all observations, the mean difference between the two rheologies is small. The drift speeds simulated using the viscous-plastic rheology are closest to the buoy-measured and remotely-sensed drift speeds.

Divergence rates estimated using optimally-interpolated AVHRR and SAR-derived motion fields are similar and show considerable local variability within a mean converging field. Simulated divergence rates overestimate convergence relative to the observations, although both observed and modeled rates are small. Localized changes in SSM/I-derived concentrations are typically consistent with regions of convergence and divergence in the pack. Significant correlations were found in some areas between changes in SSM/I-derived concentrations and simulated divergence and shear over about 40% of the study area.

Enough uncertainties exist regarding data sets, algorithms, and definitions that the absolute amount of open-water production in relation to atmospheric synoptic systems cannot be determined unambiguously. The effects of such differences in retrieved concentrations, when considered in terms of turbulent flux estimates, show substantial differences depending on the data type and classification scheme used to retrieve ice concentrations.

To further define ice-pack responses to atmospheric conditions, work is underway to extend these case studies in combination with surface and aircraft observations, and to build a long-term time series of remotely-sensed ice concentrations, ice motion, and simulations using different modeling options. In addition to specifying the requirements of remote sensing systems and field programs for sea-ice applications, such work should assist in the eventual assimilation of such merged data sets into operational ice models, and should aid in testing simplifications desirable for climate modeling applications.

## 3. YEAR 4 PLANS

### 3.1 Ice Type Classification

We do not anticipate significant further work on comparing SAR and TM-derived ice type classification with SAR. Possible investigations, if time allows, include the use of texture and other spatial information, along with single and multiple channel images, in the ice typing process.

### 3.2 Seasonal Cycle Study

The seasonal cycle study is a major focus of our work, and will be continued. The assumptions used in the simple ice cover/backscatter model will be reexamined, and runs will be made with different values for some parameters (for example, the backscatter and fractional coverage of wet snow and meltponds). Results of our other work on the backscatter of new ice and YI will be included to study the effects of these types on the mean backscatter from the SAR scenes. We intend to investigate the effects of using image-dependent thresholds for ice types rather than the global thresholds currently in use. Finally, we will explore the inclusion of a more complex sea ice backscatter model instead of the extremely simple backscatter model used so far.

### 3.3 Ice Concentration

The ice concentration algorithm we have developed would benefit from further investigation. We plan to study the inclusion of the thinner ice types (NI, grey ice, and grey-white ice) in the algorithm as well as the use of multitemporal information to further constrain the problem. The use of an estimated lead formation rate may be a promising approach to improvement.

### 3.4 Polynya Studies

We also expect to continue our analysis of the Lady Ann Strait polynya data set. The cause of the observed backscatter trends on monthly time scales remains an open question, and we will examine and evaluate possible mechanisms. The SAR "snapshots" of the polynya, while not suitable for a rigorous study of ice dynamics within the polynya, may be useful for validating a coupled ice/ocean polynya model currently under development by J. Heinrichs.

## 4. REFERENCES


Barry, R.G. and J.A. Maslanik, 1989, Arctic Sea Ice Characteristics and Associated Atmosphere-Ice Interactions. *Geojournal*, Vol. 18.1, pp. 35-44.

Center for the Study of Earth from Space, 1991, *Spectral Image Processing System User's Guide*, CSES, CIRES, University of Colroado, Boulder, October 1991.

Heinrichs, J., J. Maslanik, and K. Steffen, 1994, A Seasonal Study of Sea Ice in the Beaufort Sea Using ERS-1 SAR Data, *Journal of Geophysical Research*, submitted.

Hibler, W. D., 1985, Modeling Sea-ice Dynamics, *Advances in Geophysics*, 28A: 549-579.

Ito, H., 1981, *Sea Ice Atlas of Northern Baffin Bay*, Zürcher Geographische Schriften, No. 7, ETH, Zurich.

Kwok, R., and G. Cunningham, 1992, *Geophysical Processor System Data User's Handbook*, NASA, JPL, Pasadena, CA, JPL D-9526 (draft).

Kwok, R., E. Rignot, B. Holt, and R. Onstott, 1992, Identification of Sea Ice Types in Spaceborne Synthetic Aperture Radar Data, *Journal of Geophysical Research*, 97(C2).

Steffen, K., and A. Schweiger, 1990, A Multisensor Approach to Sea Ice Classification for the Validation of DMSP-SSM/I Passive Microwave Derived Sea Ice Products, *Photogrammetric Engineering and Remote Sensing*, 56(1): 75-82.

Steffen, K., and A. Schweiger, 1991, NASA Team Algorithm for Sea Ice Concentration Retrieval from Defense Meteorological Satellite Program Special Sensor Microwave Imager: Comparison With Landsat Satellite Imagery, *Journal of Geophysical Research*, 96(C12): 21971-21987.

Steffen, K., and J. Heinrichs, 1994a, Feasibility of Sea Ice Typing with Synthetic Aperture Radar: Merging of Landsat Thematic Mapper and ERS-1 SAR Satellite Imagery, *Journal of Geographical Research*, in press.

Steffen, K., and J. Heinrichs, 1994b, Variability of Young Ice in the Lady Ann Strait Polynya Observed with the ERS-1 SAR, *Journal of Geophysical Research*, in preparation.

Wismann, V., A C-band Wind Scatterometer Model Derived from the Data Obtained During the ERS-1 Calibration/Validation Campaign, 1993, *Proceedings First ERS-1 Symposium*, Cannes, France, 4-6 November 1992, ESA SP-359, 55-59.

WMO, 1970, *Sea Ice Nomenclature*, WMO/OMM/BMO, No. 259, Geneva.

## 5. PUBLICATIONS SUPPORTED BY NAGW-2598

Fowler, C., J. A. Maslanik, and W. J. Emery, 1994, Observed and simulated responses of a high-concentration ice cover to synoptic weather systems, *Journal of Geophysical Research*, (submitted).

Heinrichs, J., J. Maslanik, and K. Steffen, 1994, A Seasonal Study of Sea Ice in the Beaufort Sea Using ERS-1 SAR Data, *Journal of Geophysical Research*, submitted.

Maslanik, J. A. and H. Maybee, 1994. Assimilating remotely-sensed data into a dynamic-thermodynamic sea ice model, IGARSS '94, in press.

Maslanik, J. A., C. Fowler, J. Heinrichs, R. G. Barry, and W. J. Emery, 1994, Remotely-sensed and simulated variability of Arctic sea-ice concentrations in response to atmospheric synoptic systems, *International Journal of Remote Sensing*, (submitted).

Steffen, K., J. Heinrichs, J. Maslanik, and J. Key, 1993, Sea ice feature and type identification in merged ERS-1 SAR and Landsat Thematic Mapper Imagery, *Proceedings First ERS-1 Symposium*, ESA SP-359, Cannes, France, October, 1992.

Steffen, K., and J. Heinrichs, 1994, Feasibility of Sea Ice Typing with Synthetic Aperture Radar: Merging of Landsat Thematic Mapper and ERS-1 SAR Satellite Imagery, *Journal of Geographical Research*, in press.

Steffen, K., and J. Heinrichs, 1994, Variability of Young Ice in the Lady Ann Strait Polynya Observed with the ERS-1 SAR, *Journal of Geophysical Research*, in preparation.

## 6. ACRONYM LIST

| | |
|---|---|
| ASF | Alaska SAR Facility |
| BI | Bright Ice |
| CU | University of Colorado |
| EOSAT | Earth Observation Satellite Corporation |
| ERS-1 | Earth Resources Satellite - 1 |
| FYI | First-year Ice |
| GPS | Geophysical Processor System |
| IC | Ice Concentration |
| IF | Ice Free |
| IDL | Interactive Data Language |
| MYI | Multiyear Ice |
| NI | Nilas |
| NMC | National Meteorological Center |
| OI | Old Ice |
| SAR | Synthetic Aperture Radar |
| SIPS | Spectral Image Processing System |
| SSM/I | Special Sensor Microwave Imager |
| TM | Thematic Mapper |
| UTM | Universal Transverse Mercator |
| WMO | World Meteorological Organization |
| YI | Young Ice |